

Entrance channel effects on the evaporation residue yields in reactions leading to the ^{220}Th compound nucleus

Kyungil Kim and Youngman Kim

*Rare Isotope Science Project, Institute for Basic Science, Daejeon 305-811, Korea**

Avazbek Nasirov

Joint Institute for Nuclear Research, Joliot-Curie 6, 141980 Dubna, Russia and

Institute of Nuclear Physics, Ulugbek, 100214, Tashkent, Uzbekistan[†]

Giuseppe Mandaglio

Dipartimento di Fisica e di Scienze della Terra dell'Università di Messina,

Salita Sperone 31, 98166 Messina, Italy

Istituto Nazionale di Fisica Nucleare, Sezione di Catania, Italy and

Centro Siciliano di Fisica Nucleare e Struttura della Materia 95125 Catania, Italy

Giorgio Giardina

Dipartimento di Fisica e di Scienze della Terra dell'Università di Messina,

Salita Sperone 31, 98166 Messina, Italy and

Istituto Nazionale di Fisica Nucleare, Sezione di Catania, Italy

(Dated: June 13, 2021)

The evaporation residue yields from compound nuclei ^{220}Th formed in the $^{16}\text{O}+^{204}\text{Pb}$, $^{40}\text{Ar}+^{180}\text{Hf}$, $^{82}\text{Se}+^{138}\text{Ba}$, $^{124}\text{Sn}+^{96}\text{Zr}$ reactions are analyzed to study the entrance channel effects by comparison of the capture, fusion and evaporation residue cross sections calculated by the combined dinuclear system (DNS) and advanced statistical models. The difference between evaporation residue (ER) cross sections can be related to the stages of compound nucleus formation or/and at its surviving against fission. The sensitivity of the both stages in the evolution of DNS up to the evaporation residue formation to the angular momentum of DNS is studied. The difference between fusion excitation functions are explained by the hindrance to complete fusion due to the larger intrinsic fusion barrier B_{fus}^* for the transformation of the DNS into a compound nucleus and the increase of the quasifission contribu-

tion due to the decreasing of quasifission barrier B_{qf} as a function of the angular momentum. The largest value of the ER residue yields in the very mass asymmetric $^{16}\text{O}+^{204}\text{Pb}$ reaction is related to the large fusion probability and to the relatively low threshold of the excitation energy of the compound nucleus. Due to the large threshold of the excitation energy (35 MeV) of the $^{40}\text{Ar}+^{180}\text{Hf}$ reaction, it produces less the ER yields than the almost mass symmetric $^{82}\text{Se}+^{138}\text{Ba}$ reaction having the lowest threshold value (12 MeV).

PACS numbers: 25.70.Jj, 25.70.Gh

I. INTRODUCTION

The continuance and complexity of processes preceding the formation of the reaction products in heavy ion collisions at low energies are of interest in the theoretical and experimental studies. Due to very transiency of these processes it is impossible to observe how they occur. The comprehension about the role of the shape and structure of the colliding nuclei in formation of the observed products can be established by the comparison of the experimental data obtained for the reactions with the different projectile- and target-nucleus leading to the formation of the same compound nucleus (CN) [1–6]. In all of these works, the results of the comparisons led to the same conclusions: the evaporation residue (ER) cross sections of the same heated and rotating CN are different even at the same value of the excitation energy E_{CN}^* . The main conclusion of the authors in interpretations of the observed differences between ER cross sections is an appearance of the hindrance to complete fusion in the stage of the CN formation. In eighties the extra-extra-push model, the surface friction model and “dissipative-diabatic-dynamics” model were applied to reproduce the mean values of the barrier of the reaction [1]. In these studies the role of the orbital angular momentum in the mechanism of the DNS formation and its transformation into CN was not considered. The extent of the hindrance is determined by the peculiarities of the potential energy surface [3–6] which contains shell effects of the intrinsic structure of interacting nuclei. The hindrance to complete fusion is related with the increase of the

* kyungil@ibs.re.kr

† nasirov@jinr.ru

quasifission events in the evolution of the DNS formed at capture of the projectile by the target. Theoretical studies of the appearance of the quasifission products showed that their yield and mass distribution are determined by the mass (charge) asymmetry of the entrance channel and peculiarities of the potential energy surface. In Ref. [6], the observed fact that the ER cross section of the $^{124}\text{Sn}+^{92}\text{Zr}$ reaction is larger than the one of the more mass asymmetric $^{86}\text{Kr}+^{130}\text{Xe}$ reaction was explained with the higher value of the potential energy surface corresponding to the former reaction than the one of the latter reaction.

In this work, we have calculated and compared the capture, fusion and ER cross sections of the four reactions forming ^{220}Th which have different mass asymmetries: $^{16}\text{O}+^{204}\text{Pb}$, $^{40}\text{Ar}+^{180}\text{Hf}$, $^{82}\text{Se}+^{138}\text{Ba}$, and $^{124}\text{Sn}+^{96}\text{Zr}$. The role of the orbital angular momentum in the formation of a compound nucleus is demonstrated.

II. OUTLINE OF THE APPROACH

The study of the main processes taking place in heavy ion collisions at the near Coulomb barrier energies is based on the calculations of the incoming path of projectile-like nucleus on the target-nucleus and finding capture probability taking into account the possibility of interaction with different orientation angles of the axial symmetry axis of deformed nuclei [7–9]. Also the surface vibration of the non-deformed nuclei is taken into consideration. Capture of the projectile by the target-nucleus is characterized by the full momentum transfer of the relative momentum into the intrinsic degrees of freedom and shape deformation. The capture occurs, if the following necessary and sufficient conditions are satisfied. The necessary condition of capture is overcoming the Coulomb barrier by projectile nucleus to be trapped in the potential well of the potential energy surface. But, overcoming the Coulomb barrier by the projectile is not enough to be trapped. The condition of sufficiency for capture is the decrease of the relative kinetic energy due to dissipation by friction forces up to values lower than the depth of the potential well [6, 7, 10]. It depends on the values of the beam energy and orbital angular momentum, the size of the potential well and intensity of the friction forces that cause dissipation of the kinetic energy of the relative motions to internal energy of two nuclei. So, the trapping of the collision path into the well is a capture process. In Fig. 1, on the potential energy surface (PES), this process is showed by the dashed arrow (a).

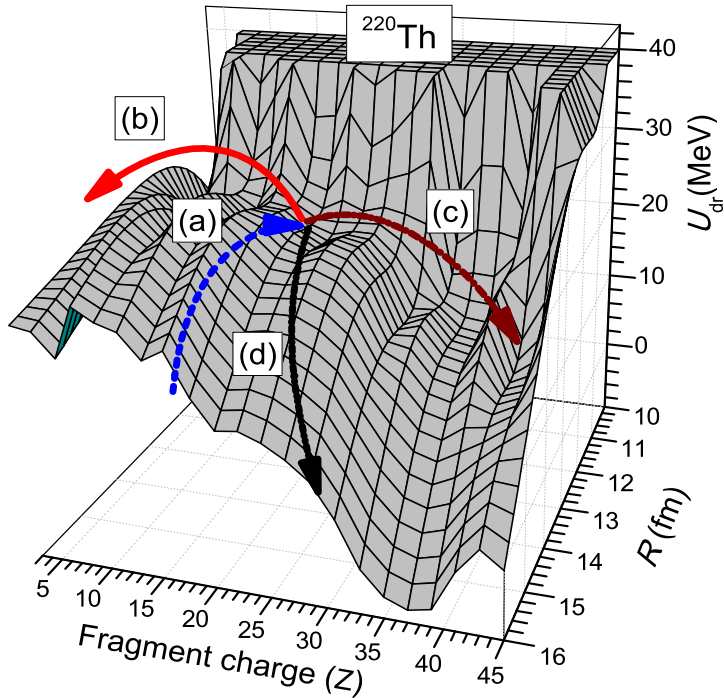


FIG. 1. (Color online) Potential energy surface calculated as a function of the relative distance between nuclei and charge number of a fragment for reactions leading to the ^{220}Th CN. Arrow (a) shows the capture path in the entrance channel; arrow (b) shows the direction of the complete fusion by multinucleon transfer from the light nucleus to the heavy one; (c) and (d) arrows show the directions of decay of the DNS into mass symmetric and asymmetric quasifission channels, respectively.

The PES is calculated for the corresponding values of angular momentum (ℓ) and orientation angles α_1 and α_2 of the colliding nuclei by the following expression:

$$\begin{aligned}
 U(A, Z, \ell, R, \alpha_1; \alpha_2) \\
 = B_1 + B_2 + V(A, Z, \ell, \alpha_1; \alpha_2; R) - (B_{CN} + V_{rot}^{CN}(\ell)),
 \end{aligned}
 \tag{1}$$

where $Z = Z_1$ is charge number of the DNS fragment; $Z_2 = Z_{\text{tot}} - Z_1$, Z_{tot} is the total charge number of interacting nuclei; R is the distance between centres of interacting nuclei; B_1 , B_2 and B_{CN} are the binding energies of the projectile, the target and the CN, respectively. The peculiarities of the DNS evolution is determined by the landscape of the PES which changes strongly with the increasing the total charge and mass numbers of the CN. The solid arrow (b) in Fig. 1 shows the evolution of the system to complete fusion while the

dot-dashed (c) and dot-dot-dashed (d) arrows show the decay of DNS forming projectile-like (target-like) products and the decay from more mass symmetric configurations, respectively. The stability of DNS against decay into two fragments is determined by the depth of the potential well which is formed due to attractive nucleus-nucleus interaction. Therefore, the depth of the potential well is called quasifission barrier. Only part of the paths of the DNS evolution along the solid arrow (b) and surviving against decay along the relative distance lead to complete fusion, *i.e.* to the CN formation. The fusion probability P_{CN} is used to take into account the competition between the complete fusion and decay of DNS into two fragments (quasifission) to calculate complete fusion cross section [6, 7]:

$$\sigma_{fus}(E) = \sum_{\ell=0}^{\ell_d(E)} (2\ell + 1) \sigma_{cap}(E, \ell) P_{CN}(E, \ell). \quad (2)$$

The maximum values of ℓ leading to capture $\ell_d(E)$ is calculated by the solution of the radial motion equations (see Ref. [7]). We should stress its dependence on the collision energy of nuclei. The decay of DNS without reaching the CN shape is called quasifission. Its cross section is calculated by the expression

$$\sigma_{qfis}(E) = \sum_{\ell=0}^{\ell_d} (2\ell + 1) \sigma_{cap}(E, \ell) (1 - P_{CN}(E, \ell)). \quad (3)$$

The details of calculation of the capture, fusion and ER cross sections can be found in Refs. [6, 7].

A. Deformed nuclei

The expectation values of the capture and fusion cross sections are obtained by averaging contributions of different orientation angle, α , which is the angle of the nucleus relatively to the beam direction at the initial stage of reaction:

$$\langle \sigma_i(E_{c.m.}) \rangle = \int_0^{\pi/2} \sin \alpha \sigma_i(E_{c.m.}; \alpha) d\alpha \quad (4)$$

Deformation parameters of the ground quadrupole and octupole states are obtained from Ref. [11] of the reacting nuclei in this work while the ones of the first excited first 2^+ and 3^- states are obtained from Refs. [12] and [13], respectively.

TABLE I. Deformation parameters of the ground state, first excited 2^+ and 3^- states used in the calculations in this work.

Nucleus	β_2	β_3	β_{2+} [12]	β_{3-} [13]
^{16}O	0.021	0.0	0.364	0.37
^{204}Pb	-0.008	0.0	0.41	0.114
^{40}Ar	0.0	0.0	0.284	0.26
^{180}Hf	0.279	0.0	0.274	0.07
^{82}Se	0.154	0.0	0.193	0.161
^{138}Ba	0.0	0.0	0.093	0.118
^{124}Sn	0.0	0.0	0.095	0.27
^{96}Zr	0.217	0.0	0.080	0.133

B. Surface vibration

The surface vibrations are regarded as independent harmonic vibrations and the nuclear radius is considered to be distributed as a Gaussian distribution [14],

$$g(\beta_2, \beta_3) = \exp \left[-\frac{(\sum_{\lambda} \beta_{\lambda} Y_{\lambda 0}^*(\alpha))^2}{2\sigma_{\beta}^2} \right] (2\pi\sigma_{\beta}^2)^{-1/2}, \quad (5)$$

where α is the direction of the spherical nucleus. For simplicity, we use $\alpha = 0$.

$$\sigma_{\beta}^2 = R_o^2 \sum_{\lambda} \frac{2\lambda + 1}{4\pi} \frac{\hbar}{2D_{\lambda}\omega_{\lambda}} = \frac{R_o^2}{4\pi} \sum_{\lambda} \beta_{\lambda}^2, \quad (6)$$

where $R_o = 0.917\sqrt{(R_p^2 + R_n^2)}$, R_p and R_n are the proton and neutron distribution radii, respectively. R_p and R_n are calculated by the expressions from Ref. [15]:

$$R_p = 1.237(1. - 0.157(1 - 2\frac{Z}{A}) - 0.646\frac{1}{A})A^{1/3} \quad (7)$$

$$R_n = 1.176(1. + 0.250(1 - 2\frac{Z}{A}) + 2.806\frac{1}{A})A^{1/3}. \quad (8)$$

$$\langle \sigma_i(E_{c.m.}) \rangle = \int_{-\beta_{2+}}^{\beta_{2+}} \int_{-\beta_{3-}}^{\beta_{3-}} \sigma_i(E_{c.m.}) \cdot g(\beta_2, \beta_3) d\beta_2 d\beta_3 \quad (9)$$

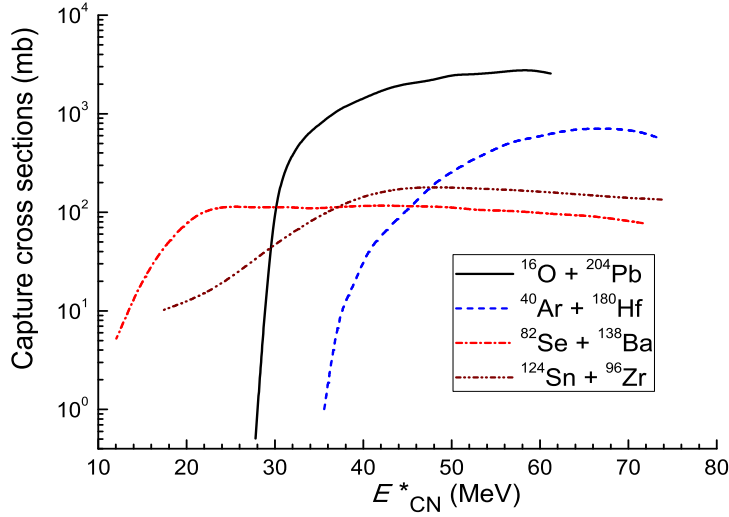


FIG. 2. (Color online) Comparison of the capture excitation functions calculated in this work for the $^{16}\text{O}+^{204}\text{Pb}$ (solid line), $^{40}\text{Ar}+^{180}\text{Hf}$ (dashed), $^{82}\text{Se}+^{138}\text{Ba}$ (dot-dashed), and $^{124}\text{Sn}+^{96}\text{Zr}$ (dot-dot dashed) reactions.

III. RESULTS AND DISCUSSION

A. Comparison of capture and fusion cross-sections

The influence of peculiarities of the entrance channel on the characteristics of the formed reaction products can be studied by the comparison of the experimental data and theoretical results obtained for the reactions leading to the formation of the same CN. The comparison of the capture and fusion cross sections obtained for the $^{16}\text{O}+^{204}\text{Pb}$, $^{40}\text{Ar}+^{180}\text{Hf}$, $^{82}\text{Se}+^{138}\text{Ba}$, and $^{124}\text{Sn}+^{96}\text{Zr}$ reactions are presented in Figs. 2 and 3, respectively.

Hereafter the CN excitation energy E_{CN}^* is used instead of the collision energy in the center-of-mass system $E_{\text{c.m.}}$ for the convenience of comparison of the reactions having large difference in the Coulomb barrier energies. The threshold values of E_{CN}^* for the capture excitation functions is determined by the Coulomb barriers of the entrance channel and by the reaction Q_{gg} -value:

$$E_{\text{CN}}^*(Z = Z_1) = E_{\text{c.m.}}^{(\min)}(Z) + Q_{\text{gg}}(Z) = V_B^{(\text{Coul})}(Z) + Q_{\text{gg}}(Z). \quad (10)$$

Due to large values of $Q_{\text{gg}} = -180.516$ MeV and -188.332 MeV for $^{82}\text{Se}+^{138}\text{Ba}$ and $^{124}\text{Sn}+^{96}\text{Zr}$ reactions, respectively, the entrance channel positions are at valleys of the PES corresponding to $Z = 34$ and 40 . Their positions on the PES are lower in comparison with the ones for the

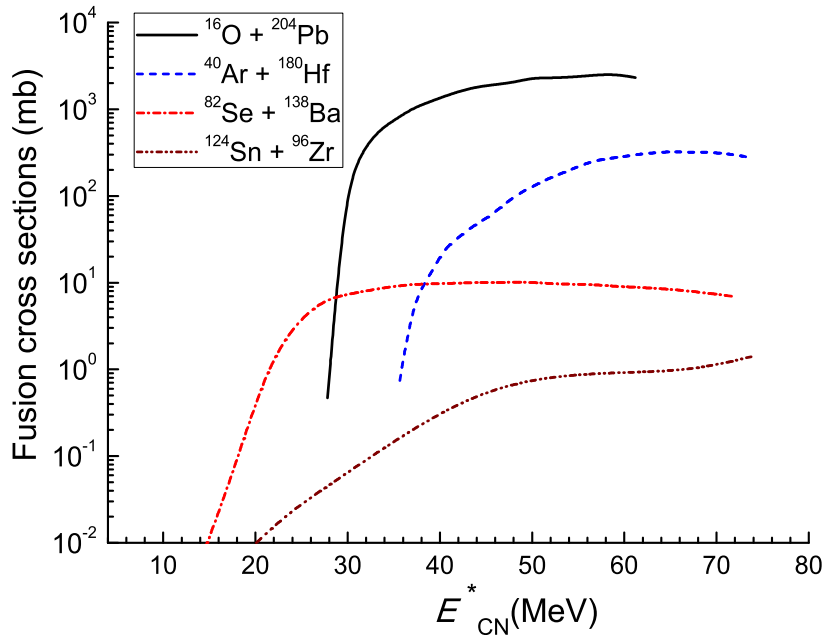


FIG. 3. (Color online) Comparison of the fusion excitation functions calculated in this work for the $^{16}\text{O}+^{204}\text{Pb}$ (solid line), $^{40}\text{Ar}+^{180}\text{Hf}$ (dashed), $^{82}\text{Se}+^{138}\text{Ba}$ (dot-dashed), and $^{124}\text{Sn}+^{96}\text{Zr}$ (dot-dot dashed) reactions.

$^{16}\text{O}+^{204}\text{Pb}$ and $^{40}\text{Ar}+^{180}\text{Hf}$ reactions which are placed at $Z = 8$ and 18. So, the difference of the $U(Z, R)$ values as a function of Z appears as a difference in the threshold values of E_{CN}^* at which capture occurs.

The capture excitation functions obtained for the mass asymmetric $^{16}\text{O}+^{204}\text{Pb}$ and $^{40}\text{Ar}+^{180}\text{Hf}$ reactions are one order of magnitude higher than the ones for the almost symmetric $^{82}\text{Se}+^{138}\text{Ba}$ and $^{124}\text{Sn}+^{96}\text{Zr}$ reactions. This strong difference in the capture cross sections is related with the size of the potential well in the nucleus-nucleus interaction. The Coulomb repulsion is stronger for the almost symmetric reactions in comparison with the one for the asymmetric reactions: $(Z_1 \cdot Z_2)_{\text{asym}} < (Z_1 \cdot Z_2)_{\text{sym}}$. Therefore, strong repulsion forces make the potential well shallower, reducing consequently the maximum number of the partial waves ($\ell_d(E)$) leading to capture, and the capture cross section decreases (see Eq. 2).

The excitation functions of complete fusion calculated for the reactions under study are compared in Fig. 3. The fusion excitation function of the almost symmetric reaction is even two orders of magnitude lower than the one of the mass asymmetric reaction. In the

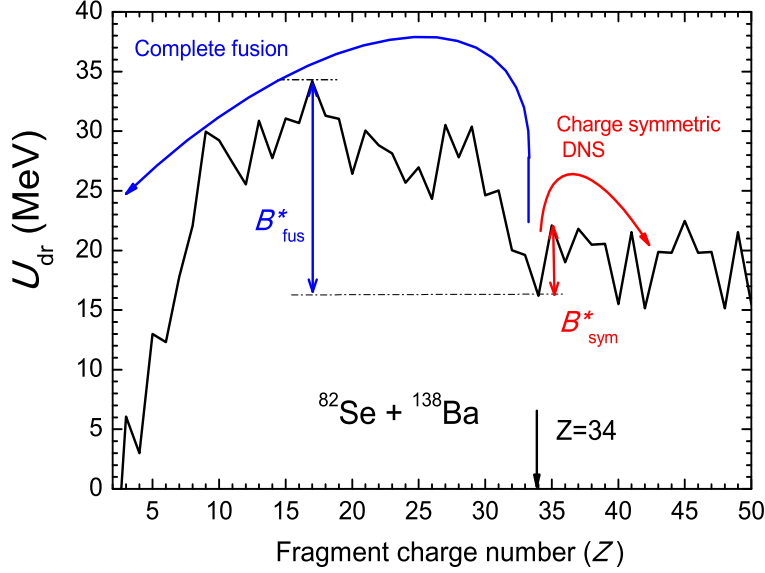


FIG. 4. (Color online) Driving potential of the DNS leading to formation of the ^{220}Th compound nucleus. The barriers B_{fus}^* and B_{sym}^* make hindrance to the evolution of the DNS to complete fusion and to reach its symmetric configurations, respectively, in the case of the $^{82}\text{Se}+^{138}\text{Ba}$ reaction ($Z=34$).

framework of the model used in this work, this result is explained by the hindrance to complete fusion due to the larger intrinsic fusion barrier B_{fus}^* for the transformation of the DNS into the CN and smaller quasifission barrier B_{qf} against its decay into two fragments for the case of more mass symmetric reactions. The height of B_{fus}^* depends on the charge and mass asymmetry of the DNS fragments and Q_{gg} -value of the reaction (see Fig. 4).

In Fig. 4 we illustrate the determination of B_{fus}^* and B_{sym}^* for the $^{40}\text{Ar}+^{180}\text{Hf}$ reaction using the driving potential calculated for the case of $\ell=0$. These barriers cause the hindrance to the evolution of the DNS to complete fusion and to reach its symmetric configurations, respectively. It is seen that the height of B_{fus}^* is large for the $^{82}\text{Se}+^{138}\text{Ba}$ ($Z=34$) and $^{124}\text{Sn}+^{96}\text{Zr}$ ($Z=40$) reactions. The increase of the barrier B_{fus}^* for these almost symmetric reactions by the increase of ℓ will be discussed in the next Section III B.

This fact certifies that the fusion cross section of the charge symmetric reactions is always smaller than the one of the charge asymmetric reaction. The fusion probability

$$P_{\text{CN}}(E_{\text{CN}}^*) = \sigma_{\text{fus}}(E_{\text{CN}}^*)/\sigma_{\text{cap}}(E_{\text{CN}}^*) \quad (11)$$

is sensitive to the intrinsic fusion barrier B_{fus}^* and quasifission barrier B_{qf} .

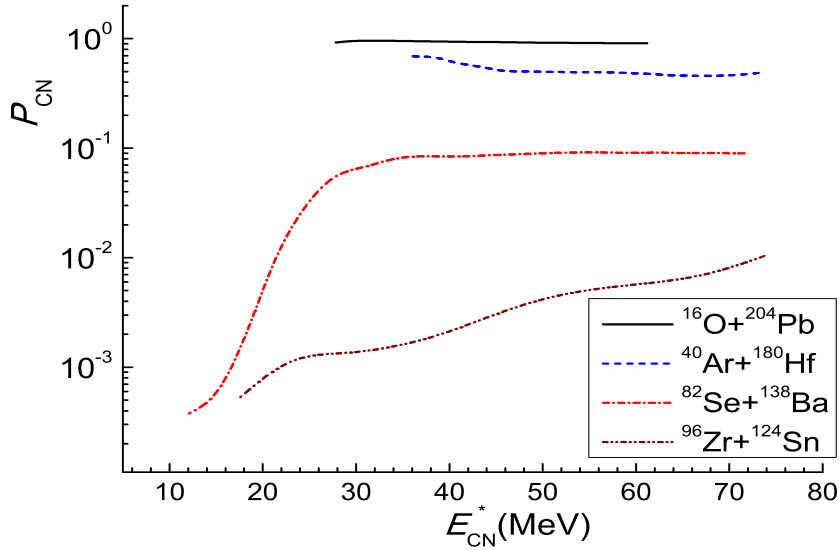


FIG. 5. (Color online) The fusion probability $P_{\text{CN}} = \sigma_{\text{fus}}/\sigma_{\text{cap}}$ calculated for the $^{16}\text{O}+^{204}\text{Pb}$, $^{40}\text{Ar}+^{180}\text{Hf}$, $^{82}\text{Se}+^{138}\text{Ba}$, and $^{124}\text{Sn}+^{96}\text{Zr}$ reactions as a function of the CN excitation energy.

Fig. 5 shows the comparison of the fusion probability P_{CN} as a function of E_{CN}^* for the four above-mentioned reactions leading to the ^{220}Th CN. The behavior of P_{CN} is different for the charge asymmetric and symmetric reactions. As one can see, P_{CN} is about 1 for the $^{16}\text{O}+^{204}\text{Pb}$ reaction (very mass asymmetric reaction) on the whole range of excitation energy E_{CN}^* . Therefore, the DNS formed in this reaction evolves almost fully to the CN. In the case of the more symmetric $^{82}\text{Se}+^{138}\text{Ba}$ and $^{124}\text{Sn}+^{96}\text{Zr}$ reactions the quasifission process is dominant in the evolution of DNS, and the fusion process is strongly hindered. The strong decrease of P_{CN} at the small values of E_{CN}^* for the mass symmetric reactions shows the presence of the large intrinsic fusion barrier which can not be overcome by the excited DNS during its evolution and it decays by quasifission channel as shown by the arrows (c) and (d) in Fig. 1.

We should stress here that the intrinsic fusion barrier B_{fus}^* is non zero at $\ell = 0$ for the heavy systems which are not very mass asymmetric. This means that the quasifission channel, which competes with complete fusion, can take place starting from $\ell = 0$ for such systems [6, 7]. This phenomenon was insinuated by the authors of Ref. [2] at comparison of the ER yields and width of fission mass distributions measured in the $^{30}\text{Si}+^{186}\text{W}$ and $^{12}\text{C}+^{204}\text{Pb}$ reactions. This conclusion is in contradiction with the well known classification of the reaction channels as function of the angular momentum. According to that classifi-

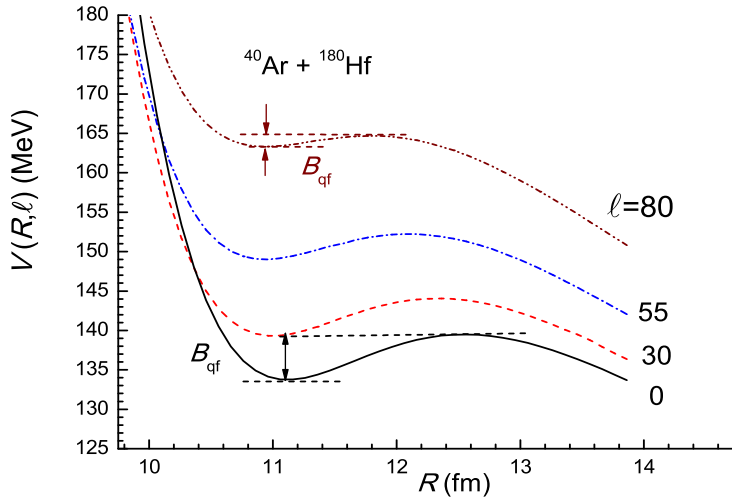


FIG. 6. (Color online) Dependence of the quasifission barrier on the angular momentum of DNS formed in the $^{40}\text{Ar} + ^{180}\text{Hf}$ reaction.

cation the complete fusion always occurs for heavy ion collisions at all values of the angular momentum $\ell < \ell_{cr}$. For the light nuclear system ℓ_{cr} is determined by the properties of the nucleus-nucleus interaction, *i.e.* by the barrier radius which is approximately equal to the sum of the radii of the target and projectile nuclei [16].

B. Role of the angular momentum in complete fusion of nuclei

The increase of beam energy from the near Coulomb barrier energies leads to increase of the number of partial waves contributing to capture and complete fusion. The change of the interaction potential due to the increase of the rotational energy by angular momentum is presented in Fig. 6 calculated for the $^{40}\text{Ar} + ^{180}\text{Hf}$ reaction. The stability of the DNS against decay is determined by the depth of the potential well, which is shown as B_{qf} depending on the angular momentum ℓ .

The partial capture cross section calculated for the $^{40}\text{Ar} + ^{180}\text{Hf}$ reaction in the range of the excitation energy $E_{CN}^* = 32\text{--}75$ MeV is presented in Fig. 7. The similar results for the $^{82}\text{Se} + ^{138}\text{Ba}$ reaction calculated in the range of the excitation energy $E_{CN}^* = 12\text{--}72$ MeV are presented in Fig. 8. Using the same scale for the partial cross section axis in the figures 7 and 8, we demonstrate the difference in the angular momentum distribution of the DNS formed in these reactions. Due to the smallness of the potential well depth for the almost

symmetric reaction we have small values of the capture cross section as it is presented in Fig. 2.

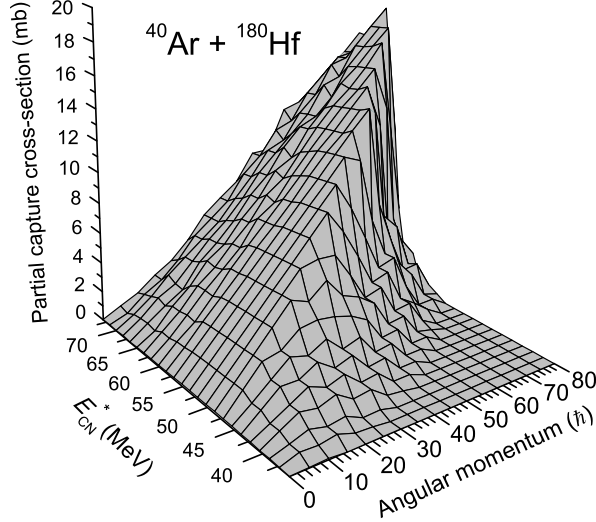


FIG. 7. Partial capture cross section of the $^{40}\text{Ar}+^{180}\text{Hf}$ reaction.

The partial cross sections of processes are important to establish the effect of the entrance channel on the evolution of DNS formed in reactions with different mass asymmetry of colliding nuclei. It is interesting to compare the angular momentum distributions of the DNS and CN. As it was shown already in Ref. [17], the CN formed with the same excitation energy in the reactions with different mass asymmetry does not have the same partial fusion cross sections, *i.e.* angular momentum distribution of the CN will be different. This phenomenon was considered to explain the difference between the experimental values of the excitation functions of the evaporation residues formation in the $^{16}\text{O} + ^{204}\text{Pb}$ and $^{96}\text{Zr} + ^{124}\text{Sn}$ reactions leading to the same CN ^{220}Th . The first reason is related to the dependence of the height and size of the nucleus-nucleus potential well. The depth of the potential well is the quasifission barrier B_{qf} as shown in Fig. 6. The decrease of the size of potential well leads to decreasing the capture probability, consequently, the fusion probability decreases. Another crucial factor decreasing the fusion probability is an increase of the intrinsic fusion barrier by the increase of the DNS angular momentum. But this dependence can be seen from the driving potential calculated for the DNS, which is formed at capture of the projectile by the target. The change of the intrinsic fusion barrier B_{fus}^* as a function of the angular momentum ℓ of DNS is demonstrated in Fig. 9. Therefore, an increase of the beam energy allows

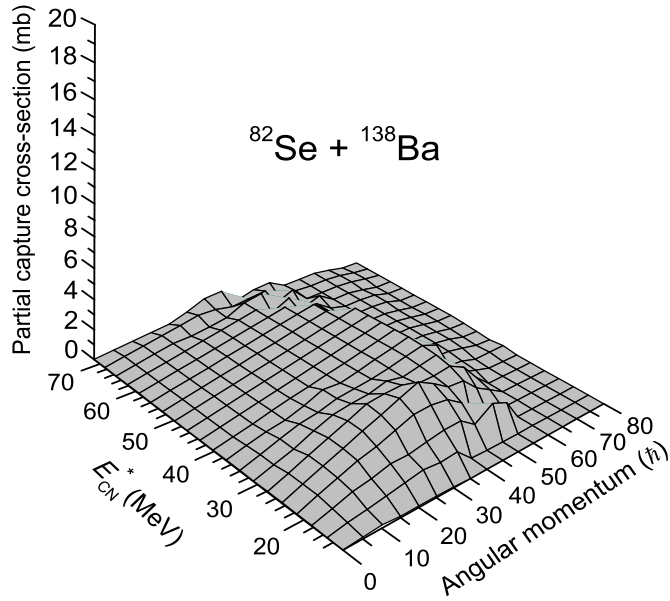


FIG. 8. Partial capture cross section of the $^{82}\text{Se}+^{138}\text{Ba}$ reaction.

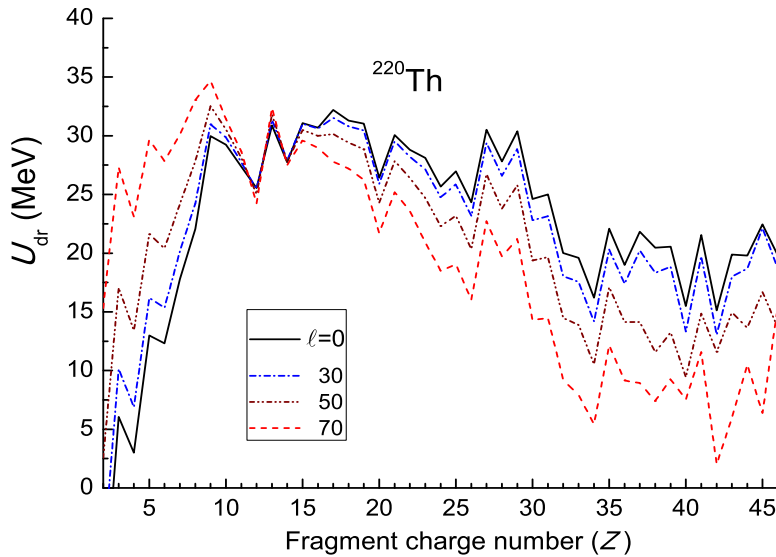


FIG. 9. (Color online) Driving potential for the dinuclear system formed in the $^{82}\text{Se}+^{138}\text{Ba}$ reaction versus the charge number of its fragment for the different values of angular momentum L .

the projectile to be trapped into the potential well with the larger values of the angular momentum which increases the capture cross section value but the P_{CN} decreases by the increase of B_{fus}^* .

The dependence of the quasifission barrier B_{qf} and intrinsic fusion barrier B_{fus}^* on the angular momentum ℓ is presented in Figs. 6 and 9, respectively. The increase of B_{fus}^*

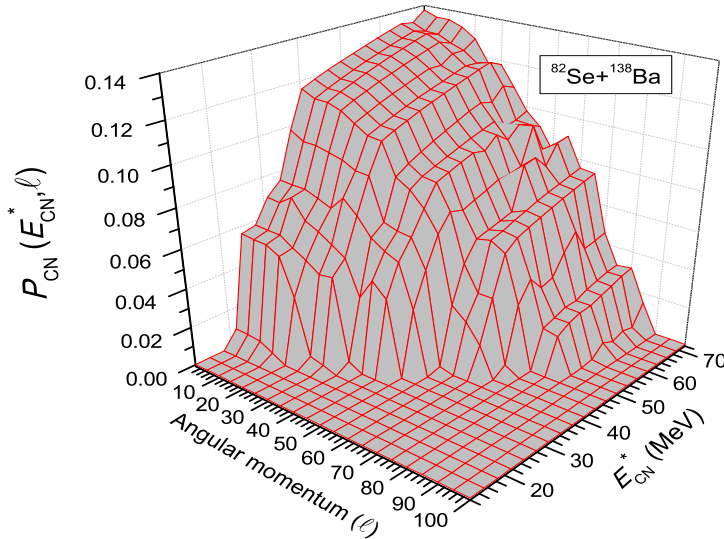


FIG. 10. (Color online) The fusion probability $P_{\text{CN}}(E_{\text{CN}}^*, \ell) = \sigma_{\text{fus}}(E_{\text{CN}}^*, \ell) / \sigma_{\text{cap}}(E_{\text{CN}}^*, \ell)$ calculated for the $^{82}\text{Se} + ^{138}\text{Ba}$ reaction as a function of the CN excitation energy and angular momentum.

decreases the probability of the CN formation. Alternative channel for the evolution of DNS is its decay into two fragments, *i.e.* quasifission. The fusion probability P_{CN} presented in Fig. 5 is found as a ratio of the summarized over angular momentum fusion and capture cross sections. It is interesting to know P_{CN} as a function angular momentum. Fig. 10 shows this dependence which is find as a ratio partial fusion and capture cross sections:

$$P_{\text{CN}}(E_{\text{CN}}^*, \ell) = \sigma_{\text{fus}}(E_{\text{CN}}^*, \ell) / \sigma_{\text{cap}}(E_{\text{CN}}^*, \ell). \quad (12)$$

The partial $P_{\text{CN}}(E_{\text{CN}}^*, \ell)$ values increase by the increase of the beam energy ($E_{\text{c.m.}} = E_{\text{CN}}^* - Q_{\text{gg}}$) but decrease by the increase of the angular momentum ℓ . We should stress that the increase of the fusion cross section is due to increase of a number of the partial waves contributing to capture and factor $(2\ell + 1)$ in calculation of the total capture cross section.

IV. COMPARISON OF THE EVAPORATION RESIDUE EXCITATION FUNCTIONS

Results of the partial cross sections of the CN formation are used to calculate evaporation residue cross sections at the given values of the CN excitation energy E_{CN}^* and angular

momentum ℓ by the advanced statistical model [18]

$$\sigma_{\text{ER}}^x(E_x^*) = \sum_{\ell=0}^{\ell_d} (2\ell + 1) \sigma_{\text{ER}}^x(E_x^*, \ell), \quad (13)$$

where $\sigma_{\text{ER}}^x(E_x^*, \ell)$ is the partial cross section of ER formation obtained after the emission of particles $\nu(x)n + y(x)p + k(x)\alpha + s(x)$ (where $\nu(x)$, y , k , and s are numbers of neutrons, protons, α -particles, and γ -quanta) from the intermediate nucleus with excitation energy E_x^* at each step x of the de-excitation cascade by formula (See Refs. [7, 18, 19]):

$$\sigma_{\text{ER}}^x(E_x^*, \ell) = \sigma_{\text{ER}}^x(E_{x-1}^*, \ell) W_{\text{sur}}^x(E_x^*, \ell). \quad (14)$$

In Eq. (14), $\sigma_{\text{ER}}^x(E_{x-1}^*, \ell)$ is the partial cross section of the intermediate excited nucleus formation at the $(x - 1)$ th step, and W_{sur}^x is the survival probability of the x th intermediate nucleus against fission along the de-excitation cascade of CN; obviously

$$\sigma_{\text{ER}}^{(0)}(E_0^*, \ell) = \sigma_{\text{fus}}(E_{\text{CN}}^*, \ell),$$

i.e., the first evaporation starts from the heated and rotating CN and $E_{\text{CN}}^0 = E_{\text{CN}}^* = E_{\text{c.m.}} + Q_{\text{gg}} - V_{\text{rot}}(\ell)$; $V_{\text{rot}}(\ell)$ is rotational energy of CN.

Due to the dependence of the fission barrier on the angular momentum ℓ [20], the survival probability $W_{\text{sur}}(E_{\text{CN}}^*, \ell)$ depends on ℓ . The damping of the shell corrections determining the fission barrier is taken into account as in Ref. [18].

Comparison of the results of ER cross sections for the four reactions under discussion allows us to reveal the role of the entrance channel properties in the formation of the reaction products. The theoretical methods applied in this work allow us to take into account the properties of the PES, peculiarities of the angular momentum distribution of the DNS and CN formed in these reactions. This circumstance is very important in order to explain the difference between the corresponding ER results. In Fig. 11 the theoretical excitation functions of the xn evaporation residues formed after neutron emission only in the $^{16}\text{O} + ^{204}\text{Pb}$ (dashed line), $^{40}\text{Ar} + ^{180}\text{Hf}$ (dot-dashed line), $^{82}\text{Se} + ^{138}\text{Ba}$ (solid line) and $^{124}\text{Sn} + ^{96}\text{Zr}$ (dotted line) reactions are compared. As it is expected, the largest cross section of the evaporation residues yield belongs to the more asymmetric $^{16}\text{O} + ^{204}\text{Pb}$ reaction, since the fusion excitation function of this reaction is highest among the others (see Fig. 3). The evaporation residue cross sections are well reproduced by the use of the angular momentum distribution of CN calculated in this work. The comparison of the theoretical excitation functions of the xn

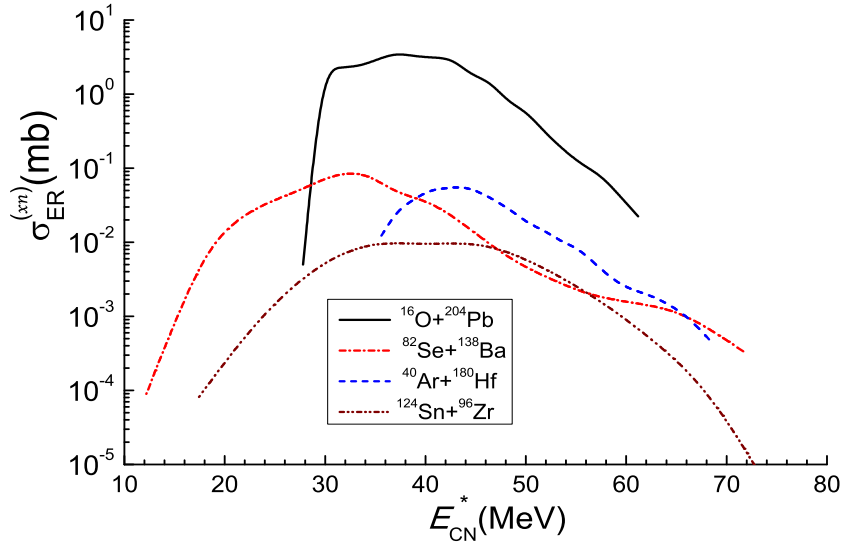


FIG. 11. (Color online) Comparison between the theoretical excitation functions of the evaporation residues formed after neutron emission only in the $^{16}\text{O}+^{204}\text{Pb}$ (dashed line), $^{40}\text{Ar}+^{180}\text{Hf}$ (dot-dashed line), $^{82}\text{Se}+^{138}\text{Ba}$ (solid line) and $^{124}\text{Sn}+^{96}\text{Zr}$ (dotted line) reactions.

ER cross sections with the experimental data of the $^{16}\text{O}+^{204}\text{Pb}$ reaction is presented in Fig. 12.

But the excitation functions of the xn evaporation residues for the $^{40}\text{Ar}+^{180}\text{Hf}$ reaction are about two orders of magnitude lower than the ones of the just discussed $^{16}\text{O}+^{204}\text{Pb}$ reaction. The main reasons causing this difference are smaller value of capture (see Fig. 2) and hindrance to complete fusion due to shell effect near ^{48}Ca .

During the evolution of the DNS formed in the $^{40}\text{Ar}+^{180}\text{Hf}$ reaction the charge and mass distributions of the system are shifted to the ^{48}Ca region. This behaviour of the center of the charge distribution is seen in Fig. 13 which shows the evolution the DNS charge distribution as a function of time. It is calculated by the method presented in Refs. [7, 10]. As a result, the intrinsic fusion barrier B_{fus}^* becomes larger causing the hindrance to complete fusion (see Fig. 9) since the driving potential has a minimum corresponding to the DNS fragment ^{48}Ca .

By increasing the beam energy the ER cross section of the $^{40}\text{Ar}+^{180}\text{Hf}$ reaction increases due to the increase capture and fusion cross sections since the partial wave numbers contributing to the capture of colliding nuclei increase. But the excitation function of the xn evaporation residues reaches maximum value at $E_{\text{CN}}^* = 44$ MeV (see Fig. 11) and then it decreases by the increase of E_{CN}^* since in this range the number of the de-excitation channels

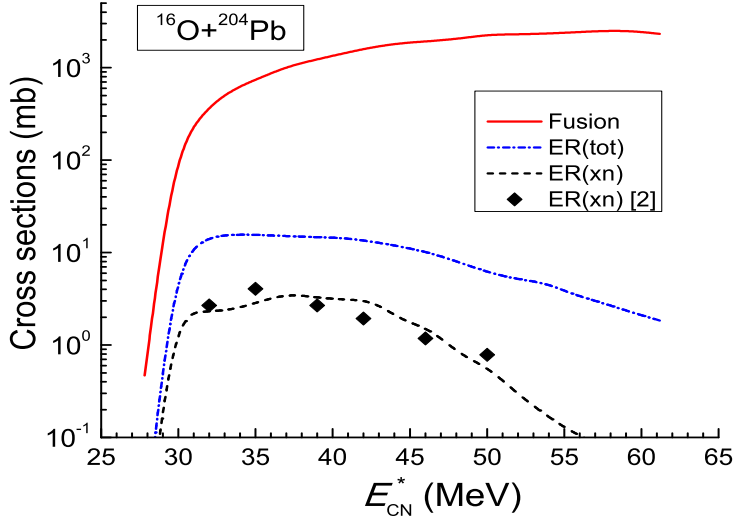


FIG. 12. (Color online) Comparison between the excitation functions of the total evaporation residues (dot-dashed line) and only neutron emission (dashed line) channels calculated for the $^{16}\text{O}+^{204}\text{Pb}$ reaction with the experimental data (diamonds) [2] of the total neutron emission channels. Solid line shows the fusion excitation function calculated in this work.

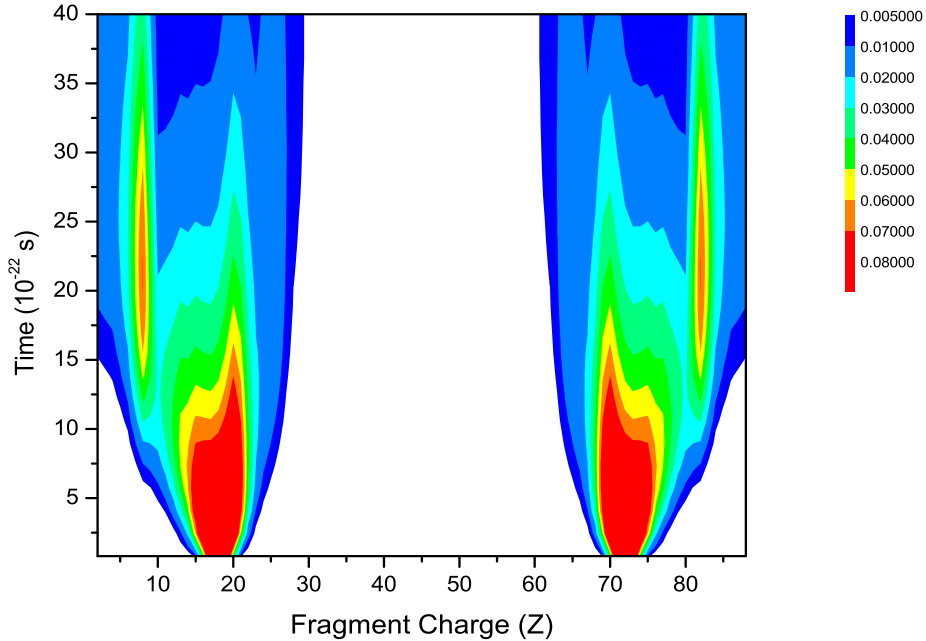


FIG. 13. (Color online) The charge distribution of the DNS fragments as a function of the interaction time for the $^{40}\text{Ar}+^{180}\text{Hf}$ reaction.

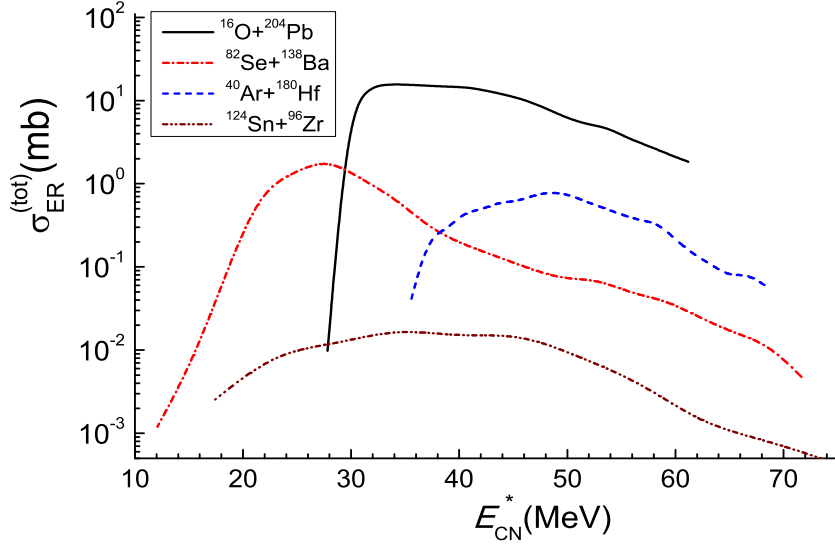


FIG. 14. (Color online) The same as in Fig. 11 but for the total evaporation residues.

increases due to the contribution of the emission of the charged particles (alpha-particle and proton). The maximum value of the total ER cross sections for the $^{40}\text{Ar}+^{180}\text{Hf}$ reaction is reached at $E_{CN}^*=50$ MeV (see Fig. 14) and then it decreases with the increase of E_{CN}^* despite the fusion cross section still increases and saturates. Such a behavior of the total ER cross section versus E_{CN}^* is related to the decrease of the survival probabilities of the intermediate excited nuclei at higher excitation energies ($E_{CN}^* > 50$ MeV) due to the increase of fission products yield. The increase of the beam energy leads to the increase of the large values of ℓ which cause decreasing the fission barrier at the beam energies corresponding to the range $E_{CN}^* > 50$ MeV. Note the $^{40}\text{Ar}+^{180}\text{Hf}$ reaction is asymmetric and due to the large size of the potential well of the nucleus-nucleus interaction the large number of partial waves contributes to the formation of the CN (see Fig. 7).

The xn and total ER excitation function for the $^{82}\text{Se}+^{138}\text{Ba}$ reaction is about one and two orders of magnitude, respectively, higher than the one of another $^{124}\text{Sn}+^{96}\text{Zr}$ reaction (see Figs. 11 and 14). Certainly, this is a result of the difference between the fusion excitation functions of these reactions (see Fig. 3). As one can see from this figure that the threshold excitation energy of fusion for the $^{82}\text{Se}+^{138}\text{Ba}$ reaction is lower than the one for the $^{124}\text{Sn}+^{96}\text{Zr}$ reaction. The fusion excitation function of the former reaction grows much faster than one for the last reaction. The slow increase of the fusion probability for the $^{124}\text{Sn}+^{96}\text{Zr}$ reaction was extracted from the analysis of the measured evaporation residues

cross sections by the authors of Ref. [1]. In our calculations we use the shape parameters corresponding to the lowest-lying 2^+ and 3^- states of projectile and target (see Table 1).

The prevalence of the ER yields cross section by the $^{82}\text{Se}+^{138}\text{Ba}$ reaction at the excitation energies $E_{\text{CN}}^* < 38$ MeV over the one in the $^{40}\text{Ar}+^{180}\text{Hf}$ reaction is seen from Figs. 11 and 14. The main significant result is related to the fact that the maximum value of the ER excitation function of the $^{82}\text{Se}+^{138}\text{Ba}$ reaction is sufficiently larger than the one of the $^{40}\text{Ar}+^{180}\text{Hf}$ reaction. It is well known that the low excitation energy E_{CN}^* is favorable for the survival probability of the heated CN against fission. But in the case of the asymmetric $^{40}\text{Ar}+^{180}\text{Hf}$ reaction the excitation energy range $E_{\text{CN}}^* < 35$ MeV is not reachable since the energy balance $Q_{\text{gg}} = -99.49$ MeV value is small. Therefore, at the beam energies $E_{\text{c.m.}} < 35 - Q_{\text{gg}}$ the capture events does not occur while for the $^{82}\text{Se}+^{138}\text{Ba}$ reaction the energy balance is $Q_{\text{gg}} = -180.52$ MeV which allows for CN to be formed with the excitation energy about 12-14 MeV. This is connected with the shell effects in colliding nuclei: ^{138}Ba has 82 (magic number) neutrons. At the beam energies corresponding to the range $E_{\text{CN}}^* > 38$ MeV the fusion cross section of the $^{40}\text{Ar}+^{180}\text{Hf}$ reaction increases sharply causing the strong increase of the ER cross sections which become higher than the ones of the $^{82}\text{Se}+^{138}\text{Ba}$ reaction. The different trends of dependence of the ER cross sections (see Fig. 14) for these two reactions in the $E_{\text{CN}}^* = 40\text{--}50$ MeV range is explained by the difference between the numbers of the partial waves contributing to the CN formation in Eq. (2) and by the decrease of the survival probabilities by increasing the CN angular momentum (see Fig. 15).

Fig. 15 shows the dependence of the survival probability as a function of the CN angular momentum and excitation energy for the $^{82}\text{Se}+^{138}\text{Ba}$ reaction. It is clearly seen that the survival probability reaches the maximum values at the low $E_{\text{CN}}^* = 21\text{--}23$ MeV excitation energies where the total ER cross section is very large since the range of the angular momentum is enough wide $\ell=0\text{--}35$. At the increase of E_{CN}^* from 20 to 70 MeV the range of the angular momentum contributing to the total ER cross section is reduced two times: mainly the range $\ell=0\text{--}18$ contributes to the results. Therefore, the total ER cross section strongly decreases in the range $E_{\text{CN}}^* = 30\text{--}70$ MeV though the fusion cross section is approximately saturated (see dot-dashed line in Fig. 3). This result shows importance of taking into account the dependence of the survival probability on the angular momentum and excitation energy of fissioning nucleus. The contribution of the angular momentum range $\ell=19\text{--}35$ to

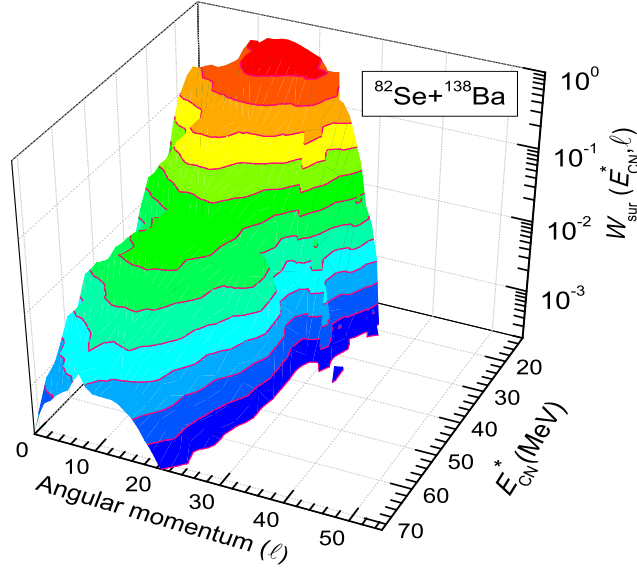


FIG. 15. (Color online) The survival probability $W_{\text{sur}}(E_{\text{CN}}^*, \ell)$ calculated for the $^{82}\text{Se}+^{138}\text{Ba}$ reaction as a function of the CN excitation energy and angular momentum.

the total ER yields is very small since fission barrier decreases by the increase of ℓ .

Nevertheless, the total ER cross sections for the $^{40}\text{Ar}+^{180}\text{Hf}$ reaction are larger than the ones of the $^{82}\text{Se}+^{138}\text{Ba}$ reaction at the larger excitation energies $E_{\text{CN}}^* > 38$ MeV. This is related with the large probability of the CN formation at large values of angular momentum which can be seen in Fig. 7. Although this figure is for the partial capture cross section, the partial fusion cross section is similar due to the large value of the fusion probability P_{CN} for $^{40}\text{Ar}+^{180}\text{Hf}$ reaction. The presence of the contribution of large values of $L = \ell\hbar$ is confirmed by the experimental data of this reaction. The larger values of the total ER cross sections measured in the experiment [21] indicate the large contribution of the alpha particle emission by CN during its de-excitation in the $E_{\text{CN}}^* > 38$ MeV range. The difference between the xn ER cross sections of these reactions is not so much since neutron emission is not sensitive to the value of angular momentum.

The individual channels of neutron emission for the $^{40}\text{Ar}+^{180}\text{Hf}$, $^{82}\text{Se}+^{138}\text{Ba}$ and $^{124}\text{Sn}+^{96}\text{Zr}$ reactions are presented in Figs. 16, 17 and 18, respectively. Peculiarities of the excitation functions of the individual de-excitation channels allow us to have information about properties of the processes during the formation of CN in these reactions. The $4n$ ER cross section is dominant in the $^{40}\text{Ar}+^{180}\text{Hf}$ reaction while the $3n$ ER channel is dominant in the $^{82}\text{Se}+^{138}\text{Ba}$ reaction. These ER channels are nearly comparable in the $^{124}\text{Sn}+^{96}\text{Zr}$ reaction.

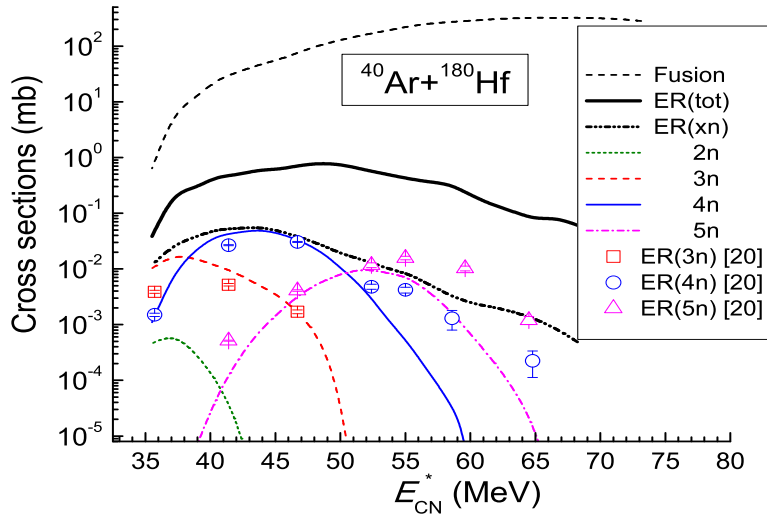


FIG. 16. (Color online) Comparison between the excitation functions of 2n (dotted line), 3n (thin dashed line), 4n (thin solid line), 5n (thin dot-dashed line) ER channels calculated in this work for the $^{40}\text{Ar}+^{180}\text{Hf}$ reaction with the ones measured in the experiment [21] for the 3n (squares), 4n (circles) and 5n (triangles) ER channels. The excitation functions of the total evaporation residues (thick solid line) and of the only neutron emission (thick dot-dashed line) channels, as well as of complete fusion (thick dashed line) calculated in this work are presented.

The threshold value of the excitation energy to complete fusion for the $^{40}\text{Ar}+^{180}\text{Hf}$ reaction is 35 MeV and, therefore, the lower energetic part of the 3n ER channel is suppressed. The fusion threshold value of E_{CN}^* of the $^{82}\text{Se}+^{138}\text{Ba}$ reaction is about 14 MeV due to the large Q_{gg} -value. Therefore, there is a favorable condition for realization of the 3n ER channel in this reaction. The results of this work show the possibility to observe 2n ER channel (thin solid curve in Fig. 17) in the $^{82}\text{Se}+^{138}\text{Ba}$ reaction.

The hindrance to complete fusion is manifested strongly in the case of more symmetric $^{124}\text{Sn}+^{96}\text{Zr}$ reaction. This phenomenon has been discussed above in relation with Figs. 2 and 3. The threshold value E_{CN}^* is about 17 MeV for this reaction, but the complete fusion excitation function increases slowly by increasing the beam energy (dot-dot-dashed curve in Fig. 3). Therefore, the 2n and 3n ER channels are open but their ER cross sections are not dominant. We have not so large difference in the maximum values of the 2n, 3n, and 4n ER cross sections for the $^{124}\text{Sn}+^{96}\text{Zr}$ reaction. The 1n and 5n ER cross sections are smaller since the 1n channel is suppressed due to fusion hindrance and the 5n channel has

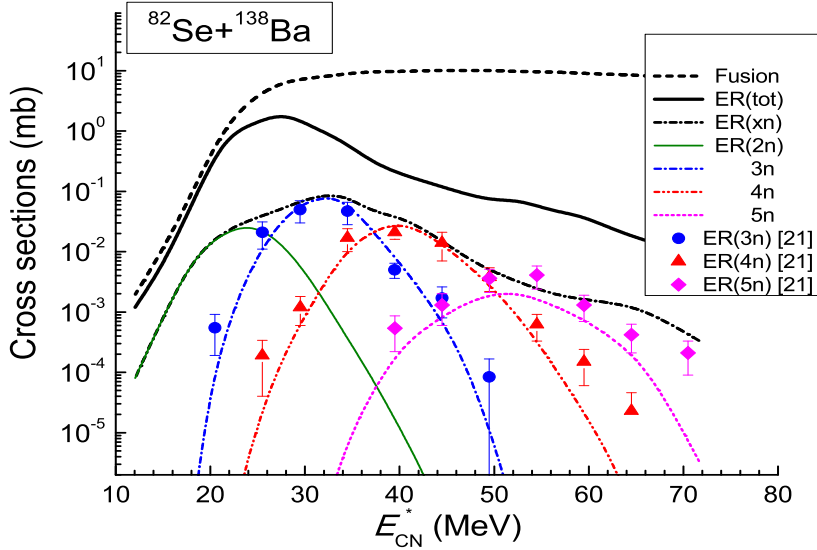


FIG. 17. (Color online) Comparison between the excitation functions of 2n (thin solid line), 3n (thin dot-dashed line), 4n (thin dot-dot-dashed line), 5n (thin dotted line) ER channels calculated in this work for the $^{82}\text{Se}+^{138}\text{Ba}$ reaction with the ones measured in the experiment [22] for the 3n (circles), 4n (triangles), and 5n (diamonds) ER channels. The excitation functions of the total evaporation residues (thick solid line) and of the only neutron emission (thick dot-dashed line) channels, as well as of complete fusion (thick dashed line) calculated in this work are presented.

very strong competition with the fission channel at large values of E_{CN}^* .

To analyze the effect of the angular momentum distribution for CN formed in different reactions we compare the partial fusion cross sections of the $^{82}\text{Se}+^{138}\text{Ba}$ and $^{124}\text{Sn}+^{96}\text{Zr}$ reactions in Figs. 19 and 20, respectively. It is seen that the main contribution of the angular momentum values is in the range $0 < L < 50\hbar$ for the CN formed in the $^{82}\text{Se}+^{138}\text{Ba}$ reaction (see Fig. 19) while this range is extended up to values $L = 70\hbar$ in the case of the $^{124}\text{Sn}+^{96}\text{Zr}$ reaction (see Fig. 20). The partial fusion cross sections of the reaction with ^{82}Se is much larger than the ones for the reaction with ^{124}Sn . Note the partial fusion cross section axis of Figs. 19 and 20 has different scale. As we discussed above (see Fig. 15), the contribution of the large values of L to the ER cross sections is small due to the strong dependence of the fission barrier on the angular momentum [18, 20]. Therefore, the ER cross sections of all these reactions analyzed in this work decrease at high values of E_{CN}^* corresponding to the beam energies sufficiently higher than the Coulomb barrier where the fusion cross section increases or reaches saturation (see Figs. 12,16,17,18). The partial fusion

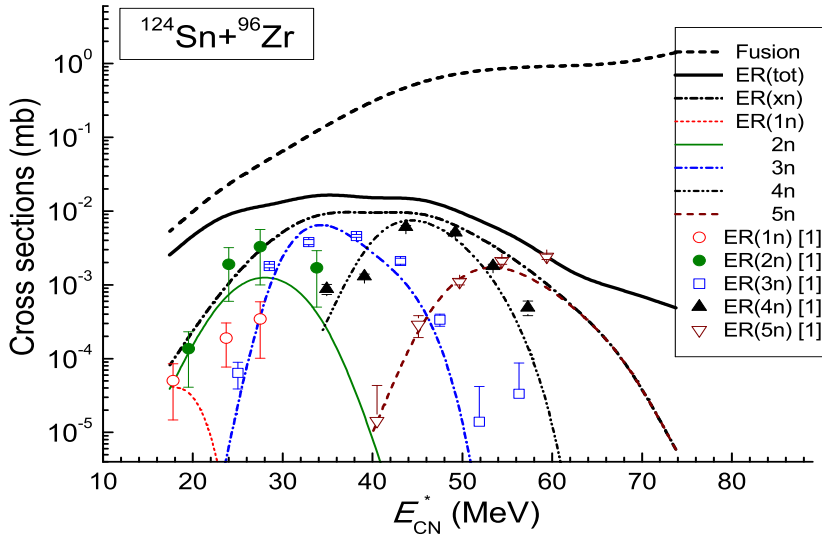


FIG. 18. (Color online) Comparison between the excitation functions of 1n (thin dotted line), 2n (solid line), 3n (thin dot-dashed line), 4n (thin dot-dot-dashed line), 5n (thin dashed line) ER channels calculated in this work for the $^{124}\text{Sn}+^{96}\text{Zr}$ reaction with the ones measured in the experiment [1] for the 1n (open circles), 2n (filled circles), 3n (open squares), 4n (filled triangles), and 5n (open triangles) ER channels. The excitation functions of the total evaporation residues (thick solid line) and of the only neutron emission (thick dot-dashed line) channels, as well as of complete fusion (thick dashed line) calculated in this work are presented.

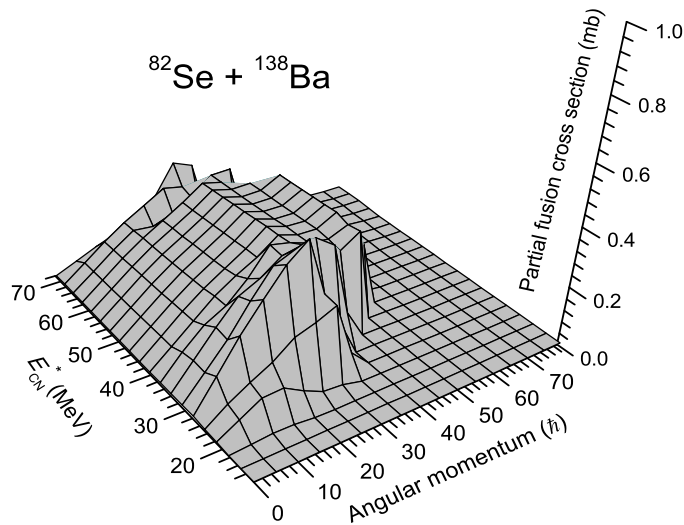


FIG. 19. Partial fusion cross section of the $^{82}\text{Se}+^{138}\text{Ba}$ reaction.

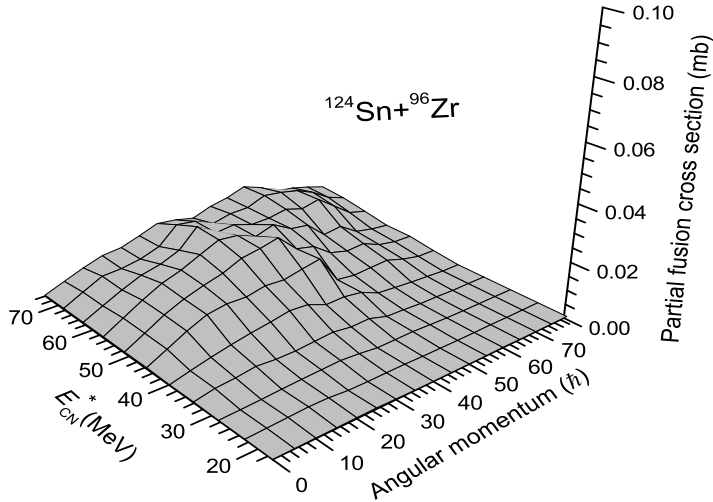


FIG. 20. Partial fusion cross section of the $^{124}\text{Sn}+^{96}\text{Zr}$ reaction.

cross sections of the $^{124}\text{Sn}+^{96}\text{Zr}$ reaction are smaller in comparison with the other reactions even at small values of E_{CN}^* .

V. CONCLUSIONS

To study the entrance channel effects on the ER yields in the reactions leading to the same CN we compare the capture, fusion and ER cross sections calculated by the combined dinuclear system and advanced statistical models. The difference between evaporation residue cross sections can be related to the stage of formation of the CN or at its surviving stage against fission by emission of neutrons and charged particles.

Comparison shows that the capture excitation functions obtained for the mass asymmetric $^{16}\text{O}+^{204}\text{Pb}$ and $^{40}\text{Ar}+^{180}\text{Hf}$ reactions are one order of magnitude higher than the ones for the almost symmetric $^{82}\text{Se}+^{138}\text{Ba}$ and $^{124}\text{Sn}+^{96}\text{Zr}$ reactions. The more strong Coulomb force makes the potential well shallower, and as a result the decrease of the number of partial waves ($\ell_d(E)$) causes decreasing the capture cross section.

The fusion excitation functions of the $^{82}\text{Se}+^{138}\text{Ba}$ and $^{124}\text{Sn}+^{96}\text{Zr}$ reactions are even two orders of magnitude lower than the ones of the mass asymmetric reactions. This result is explained by the hindrance to complete fusion due to the larger intrinsic fusion barrier B_{fus}^* for the transformation of the DNS into CN and smaller quasifission barrier B_{qf} in comparison

with values of the corresponding quantities for the more asymmetric reactions. According to our calculations B_{fus}^* increases and B_{qf} decreases by the increase of the DNS angular momentum.

Results of the partial cross sections of the CN formation are used to calculate evaporation residue cross sections at the given values of the CN excitation energy E_{CN}^* and angular momentum ℓ by the advanced statistical model. The comparison of the theoretical excitation functions of the xn evaporation residues formed in the $^{16}\text{O}+^{204}\text{Pb}$, $^{40}\text{Ar}+^{180}\text{Hf}$, $^{82}\text{Se}+^{138}\text{Ba}$ and $^{124}\text{Sn}+^{96}\text{Zr}$ reactions shows that the evaporation residue yields of the $^{16}\text{O}+^{204}\text{Pb}$ reaction is larger than the ones of the other three reactions since the fusion excitation function of this reaction is highest among the others. There is no hindrance to complete fusion.

The xn and total ER excitation functions for the almost symmetric $^{82}\text{Se}+^{138}\text{Ba}$ reaction is about one and two orders of magnitude, respectively, higher than the ones of another similar $^{124}\text{Sn}+^{96}\text{Zr}$ reaction. This is explained by the fact that the fusion excitation function of the former reaction is higher than the one of latter reaction.

The unusual prevalence of the $^{82}\text{Se}+^{138}\text{Ba}$ reaction for the ER yields in the range $E_{\text{CN}}^* < 38$ MeV in comparison with the mass asymmetric $^{40}\text{Ar}+^{180}\text{Hf}$ reaction which has larger fusion excitation function at $E_{\text{CN}}^* > 38$ MeV is analyzed. The main significant result is related to the fact that the maximum value of the ER excitation function of the $^{82}\text{Se}+^{138}\text{Ba}$ reaction is sufficiently larger than the one of the $^{40}\text{Ar}+^{180}\text{Hf}$ reaction. In the $E_{\text{CN}}^* < 35$ MeV energy range the fusion induced by ^{40}Ar is strongly hindered by the Coulomb barrier of the entrance channel. Therefore, due to relatively small Q_{gg} value (-99.49 MeV) for this reaction the lowest value of the excitation energy is $E_{\text{CN}}^* = 35$. Nevertheless, for the $E_{\text{CN}}^* > 38$ MeV energy range the total ER yields produced by the $^{40}\text{Ar}+^{180}\text{Hf}$ reaction are higher than the ones produced by the ^{82}Se induced reaction due to the strong increase of the fusion cross section of the former reaction. The total ER yields decrease with the increase of the E_{CN}^* energy for its large values is inherent for all reaction since the survival probability W_{sur} decreases due to the increase of the fission probability. At the large beam energies the number of the partial waves contributing to fusion increases causing the decrease of the fission barrier [20]. The presence of the contribution of large values of L is confirmed by the larger values of the total ER cross sections measured in the experiment [21]. The larger values of the total ER cross sections indicate the large contribution of the charged (proton and alpha) particles emission by CN during its de-excitation in the $E_{\text{CN}}^* > 38$ MeV range.

The difference between the xn ER cross sections of these reactions is not so much since neutron emission is not sensitive to the value of angular momentum.

The comparison of the $^{40}\text{Ar}+^{180}\text{Hf}$ and $^{82}\text{Se}+^{138}\text{Ba}$ reactions shows the fusion probability P_{CN} and the survival probability W_{sur} are important quantities characterizing different stages of the reaction during the formation of the CN and its surviving against fission.

The theoretical analysis of the measured data of the yield of the xn , total and individual ER residues by the combined DNS and advanced statistical models allowed us to reveal the important role of the angular momentum distribution of capture, complete fusion and de-excitation stages of the mass asymmetric and mass symmetric reactions.

ACKNOWLEDGMENTS

AKN is grateful to the Rare Isotope Science Project of the Institute for Basic Science of the Republic of Korea for supporting the collaboration between the Dubna and Daejeon groups, and thanks the Russian Foundation for Basic Research for the partial financial support in the performance of this work. This work was supported by the Rare Isotope Science Project of Institute for Basic Science funded by Ministry of Science, ICT and Future Planning and National Research Foundation of Korea (2013M7A1A1075766).

-
- [1] C.C. Sahn and H.-G. Clerc, K.-H. Schmidt, W. Reisdorf, P. Armbruster, F.P. Heßberger, J.G. Keller, G. Münzenberg, and D. Vermeulen, *Z.Phys. A* **319**, 113 (1984).
 - [2] D.J. Hinde, M. Dasgupta, and A. Mukherjee, *Phys.Rev.Lett.* **89**, 282701, 2002.
 - [3] A.Yu. Chizhov, M.G. Itkis, I.M. Itkis, G.N. Kniajeva, E.M. Kozulin, N.A. Kondratiev, I.V. Pokrovsky, R.N. Sagaidak, V.M. Voskressensky, A.V. Yeregin, L. Corradi, A. Gadea, A. Latina, A.M. Stefanini, S. Szilner, M. Trotta, A.M. Vinodkumar, S. Beghini, G. Montagnoli, F. Scarlassara, A.Ya. Rusanov, F. Hanappe, O. Dorvaux, N. Rowley, and L. Stuttge, *Phys. Rev. C* **67**, 011603(R) (2003).
 - [4] Giovanni FAZIO, Giorgio GIARDINA, Antonino L AMBERTO, Roberto RUGGERI, Carmelo SACCA, Rocco P ALAMARA , Akhtam I. M UMINOV, Avazbek K. NASIROV, Ulughbek T. YAKHSHIEV, Francis HANAPPE, Thomas MATERNA and Louise STUTTGE, *Jour. Phys.*

- Soc. of Japan, **72**, 2509 (2003).
- [5] M. Dasgupta and D.J. Hinde, Nucl. Phys. A**734**, 148 (2004).
- [6] G. Fazio, G. Giardina, G. Mandaglio, and R. Ruggeri, A.I. Muminov, A.K. Nasirov, Yu.Ts. Oganessian, A.G. Popeko, R.N. Sagaidak, and A.V. Yeremin, S. Hofmann, F. Hanappe, C. Stodel, Phys. Rev. C **72**, 064614 (2005).
- [7] Avazbek Nasirov, Akira Fukushima, Yuka Toyoshima, Yoshihiro Aritomo, Akhtam Muminov, Shuhrat Kalandarov, Ravshanbek Utamuratov, Nucl. Phys. A**759**, (2005) p.342-369.
- [8] Giovanni Fazio, Giorgio Giardina, Francis Hanappe, Giuseppe Mandaglio, Marina Manganaro, Akhtam I. Muminov, Avazbek K. Nasirov, Carmelo Sacca, Jour. Phys. Soc. of Japan, **77**, 124201, (2008).
- [9] G. Mandaglio, G. Fazio, G. Giardina, F. Hanappe, M. Manganaro, A.I. Muminov, A.K. Nasirov, and C. Sacca Physics of Atomic Nuclei, 2009, **72**, 1639 (2009).
- [10] G. Fazio, G. Giardina, G. Mandaglio, F. Hanappe, A.I. Muminov, A.K. Nasirov, W. Scheid, L. Stuttge, Mod. Phys. Lett. A 20 (2005) 391
- [11] P. Möller, J.R. Nix, W.D. Myers, and W.J. Swiatecki, Atomic Data and Nuclear Data Tables **59**, 185 (1995).
- [12] S. Raman, C. W. Nestor, JR., and P. Tikkanen, At. Data and Nucl. Data Tabl. **78**, 1 (2001).
- [13] R.H. Spear, Atomic Data and Nuclear Data Tables, **42**, 55 (1989).
- [14] H. Esbensen, Nuclear Physics A**352**, 141 (1981).
- [15] M. Warda, B. Nerlo-Pomorska, L. Pomorski, Nucl.Phys. A **635**, 484 (1998).
- [16] P. Fröbrich and R. Lipperheide, it Theory of Nuclear Reactions, (Clarendon Press, Oxford), 1996
- [17] Fazio, G. Giardina, A. Lamberto, A.I. Muminov, A.K. Nasirov, F. Hanappe, L. Stuttge, Eur. Phys. J. A 22, (2004), p.75-87
- [18] G. Mandaglio, G. Giardina, A. K. Nasirov, and A. Sobiczewski, Phys. Rev. C**86**, 064607 (2012).
- [19] G. Giardina, S. Hofmann, A.I. Muminov, A.K. Nasirov, Eur. Phys. J. A **8**, 205 (2000).
- [20] A.J. Sierk, Phys. Rev. C **33**, 2039 (1986).
- [21] D. Vermeulen, H.-G. Clerc, and C.C. Sahm, Z.Phys. A **318**, 157 (1984).
- [22] K. Satou, H. Ikezoe, S. Mitsuoka, K. Nishio, S. C. Jeong, Phys. Rev. C **65**, 054602 (2002).